Journal of Southeast University (English Edition) Vol. 29, No. 2, pp. 175 - 181 June 2013 ISSN 1003—7985

Wheel center detection based on stereo vision

Chen Xu[1] Lin Guoyu[2]

([1]School of Information and Control, Nanjing University of Information Science and Technology, Nanjing 210044, China)
([2]School of Instrument Science and Engineering, Southeast University, Nanjing 210096, China)

Abstract: As the location of the wheel center is the key to accurately measuring the wheelbase, the wheelbase difference and the wheel static radius, a high-precision wheel center detection method based on stereo vision is proposed. First, according to the prior information, the contour of the wheel hub is extracted and fitted as an ellipse curve, and the ellipse fitting equation can be obtained. Then, a new un-tangent constraint is adopted to improve the ellipse matching precision. Finally, the 3D coordinates of the wheel center can be reconstructed by the spatial circle projection algorithm with low time complexity and high measurement accuracy. Simulation experiments verify that compared with the ellipse center reconstruction algorithm and the planar constraint optimization algorithm, the proposed method can acquire the 3D coordinates of the spatial circle more exactly. Furthermore, the measurements of the wheelbase, the wheelbase difference and the wheel static radius for three types of vehicles demonstrate the effectiveness of the proposed method for wheel center detection.

Key words: wheel center; stereo vision; 3D reconstruction; ellipse stereo matching

doi: 10.3969/j.issn.1003-7985.2013.02.012

The wheel center is an important measurement parameter for measuring vehicle dimension parameters such as the wheelbase, the wheelbase difference and the wheel static radius, which can directly influence the accuracy.

Theoretically the wheel center is the center of the circular contour of a tire. So some researchers tried to handle this problem by the Hough transformation[1-4]. However, this method has some shortcomings: 1) When the optical axis of the camera is not perpendicular to the tangent plane of the tire, it is prone to generate a faked circular contour of the tire due to the tire tread; 2) The vehicle load may deform the circular contour of the tire. So the center of the rounded contour of the tire image is actually not the wheel center which cannot be extracted by detecting and fitting the rounded contour of the tire image. Furthermore, the pinhole model is one of the perspective projection transformation models, and it is not a conformal transformation. This implies that through perspective projection, the circle keeps its round shape no longer and the circle center may change its position. So the center of the fitting ellipse in image does not coincide with the projection point of the spatial circle center. For these reasons, the method using the fitting ellipse center proposed in Refs. [3, 5-6] cannot obtain the correct results.

Some scholars have done much research and proposed the following solutions:

1) The distortion error model for the circle center[7-9]. This model gives error compensation formulae which can correct the center coordinates reconstructed by two corresponding ellipse centers. However, some parameters should be known in advance, including the vector of the center, the angle of the vector etc.[7], which are difficult to acquire. So exploiting the distortion error model to compensate for errors is difficult in practice.

2) The reconstruction algorithm for spatial curve[10-14]. Due to the fact that the quadric curve pairs in stereo are the projections of a planar conic, this method globally reconstructs the conic in space by decomposing the quadric form to establish the point correspondences. This method can obtain several effective solutions, so more judgments are needed to determine which one is correct. Moreover, sometimes none of the solutions is valid because of image processing errors and calculating errors. This increases the complexity and instability of the algorithm and limits the application of the method to a certain extent.

3) Spatial circle fitting method[15-16]. This method has been widely applied to acquire the parameters of the circle including the circle center, the circle radius and the plane normal vector by constructing an optimization algorithm such as Levenberg-Marquardt. But the nonlinear optimization method may fall into a local minimum, and wrong results sometimes appear.

To solve the problems above, we propose that the wheel center be coincident with the center of the aluminum alloy wheel hub if the installation is correct. The advantages of measuring the aluminum alloy wheel hub are as follows: 1) The color and the contour of most aluminum alloy wheel hubs are well distinguished from other parts, so it is easy to locate the wheel hub; 2) From different view angles, the contour of the aluminum alloy wheel hub is elliptic. According to these, a method based

Received 2013-01-14.

Biography: Chen Xu (1979—), female, doctor, associate professor, sonia.chen@163.com.

Foundation items: The National Natural Science Foundation of China (No. 61272223), the National Key Scientific Apparatus Development of Special Item (No. 2012YQ170003-5).

Citation: Chen Xu, Lin Guoyu. Wheel center detection based on stereo vision[J]. Journal of Southeast University (English Edition), 2013, 29(2): 175-181. [doi: 10.3969/j.issn.1003-7985.2013.02.012]

on the plane projection of the spatial circle is proposed to obtain the accurate 3D coordinates of the wheel center.

1 Measurement Method for Wheel Center

In the measurement system, the basic measurement unit (BMU) composed of two cameras of the same type is a basic measurement module based on stereo vision which is used to detect the wheel center and calculate its 3D coordinates. After calibration by the 3D target, the extrinsic parameter matrices and the equation of the vehicle supporting plane can be obtained, and the BMU can figure out the 3D coordinates of the wheel center according to the geometric model.

1.1 Ellipse extraction of wheel hub contour

The image may be deformed by noise, so there may be many ellipse features in the image. In order to acquire the correct ellipse features of the wheel hub, the ellipse features possibly belonging to the wheel hub are extracted and analyzed with the prior information. The detailed process is shown below.

First, in the image preprocess, the Gaussian filter is applied to improve the image quality, then the Canny operator is used to obtain the binary edge image in which every continuous edge is checked and recorded in a chain table L_i, and finally the pixels number n_i of every continuous edge is counted. If n_i is less than the predefined threshold, this continuous edge may be noise and is removed from the binary edge image. Otherwise, the normalized ellipse fitting method is applied to calculate the ellipse fitting equation:

$$Ax^2 + Bxy + Cy^2 + Dx + Ey = 1 \tag{1}$$

where A, B, C, D, E and F are the parameters of a quadratic curve equation. Inputting all the pixels in the chain table L_i into Eq. (1) can obtain the over-determined equation solved by the singular value decomposition (SVD), and then the ellipse parameters including focus, major and minor axes are acquired.

Due to complex background and noise, there may be false edges which are similar to elliptic characteristics. In order to identify the correct edges, three ways based on the prior information are introduced to remove the false.

1) The sum of the distances from any point p_i on the ellipse to two focuses F_1 and F_2 is constant and equal to the major axis; that is $|p_iF_1| + |p_iF_2| - 2a = v_i$, where a is the length of the major axis and v_i is the residual error which should be equal to zero. In this paper, the mean of residual errors between every point in the continuous edge and the fitting ellipse can be expressed as $E = \sum v_i/n$. If E exceeds the threshold T_e, then the continuous edge is removed.

2) In the image the length of the major axis and the minor axis of the fitting ellipse for the wheel hub contour must be within a certain range.

3) For most wheels, the aluminum alloy wheel hub is light and the tire is black, so it is a good idea to extract the correct ellipse. First, the binary image is obtained through threshold segmentation in the area near the fitting ellipse. Then two discriminate conditions for the wheel hub is proposed. The gray values of most pixels in the interior of the fitting ellipse are 255 due to the light wheel hub, and the gray values of most pixels in the exterior of the fitting ellipse are 0 due to the black tire.

An algorithm based on the above information is built to eliminate the false edges caused by background and noise and extract the correct ellipse edges of the wheel hub contour.

1.2 Ellipse stereo matching with un-tangent constraint

After obtaining the ellipse edges of the wheel hub contour, the 3D coordinates of every point in the wheel hub contour can be calculated by stereo matching and 3D reconstruction. The traditional ellipse stereo matching is based on an epipolar line constraint and a sequence constraint, which means that the sequence of one point in the right epipolar line should be the same as the sequence of the same point in the left epipolar line. It is notable that a good matching result can be acquired with these two constraints except in the area where the epipolar line and the fitting ellipse are approximately tangent (see Fig. 1).

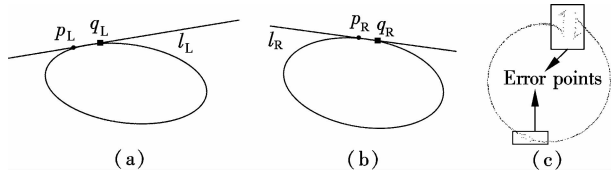

Fig. 1 Approximate tangent relationship between epipolar line and fitting ellipse. (a) Epipolar line in left image; (b) Epipolar line in right image; (c) 3D reconstruction result projected to circle plane

In Fig. 1, l_L, l_R are the epipolar lines in the left image and the right image, respectively; p_L, q_L are the intersection points of epipolar line l_L and fitting ellipse in the left image, respectively; and p_R, q_R are the intersection points of epipolar line l_R and fitting ellipse in the right image, respectively. According to the epipolar line constraint and sequence constraint, p_R and q_R are the correct correspondences of p_L and q_L, respectively. A large number of experiments have proved that in the area where the epipolar line and the fitting ellipse are approximately tangent, some correspondences may generate the wrong 3D points as shown in Fig. 1(c). Such wrong 3D points are caused by the epipolar line calculation error, the ellipse curve fitting error and the image process error.

Accordingly, a new constraint named the un-tangent constraint for the ellipse is proposed. The key is to keep away from the error prone area where the epipolar line and the fitting ellipse are approximately tangent. The un-

tangent constraint is composed of the following two constraints.

Constraint 1 The distance between the intersection points of the epipolar line and the fitting ellipse should be greater than the predefined threshold T_E, which can be calculated as

$$T_E = \begin{cases} \dfrac{M_L}{5} & |\theta_L - \theta_E| < |\theta_L - \theta_E| \\ \dfrac{M_S}{5} & |\theta_S - \theta_E| \geqslant |\theta_S - \theta_E| \end{cases} \quad (2)$$

where θ_L and θ_S are the angles of the major axis and the minor axis, respectively; θ_E is the angle of the current epipolar line; M_L and M_S are the length of the major axis and the length of the minor axis of the fitting ellipse, respectively. Eq. (2) expresses that the threshold T_E is calculated according to the length of the major axis when the current epipolar line is close to the direction of the major axis, otherwise according to the length of the minor axis.

Constraint 2 As shown in Fig. 2, the ellipse curve is divided into two parts by epipolar line l_t. Then the maximum distance from points in each ellipse part to epipolar l_t is calculated and denoted by d_1 and d_2. Suppose that $d_1 \leqslant d_2$, then d_1/d_2 should be greater than T_d (in our experiments $T_d = 0.05$).

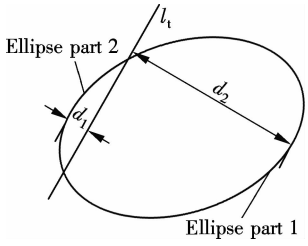

Fig. 2 Diagram of Constraint 2

So, the stereo matching process is constructed as follows:

1) Compute the intersection points between the corresponding left epipolar line and ellipse. Here p_{Li} and q_{Li} are the intersection points in the left image, and p_{Ri} and q_{Ri} are the intersection points in the right image.

2) Calculate the distance between p_{Li} and q_{Li}, and select two points with the maximum distance in the left epipolar line of the left image, denoted by p_{Lk} and q_{Lk}. The same calculation is done to p_{Ri} and q_{Ri} in the right image, denoted by p_{Rk} and q_{Rk}.

3) According to the epipolar line constraint and the sequence constraint, the corresponding points of p_{Lk}, q_{Lk}, p_{Rk} and q_{Rk} are calculated, denoted by p'_{Lk}, q'_{Lk}, p'_{Rk} and p'_{Lk}, respectively.

4) Based on the four correspondences (p_{Lk}, p'_{Lk}), (q_{Lk}, q'_{Lk}), (p_{Rk}, p'_{Rk}) and (q_{Rk}, q'_{Rk}), the correspondences of other points in ellipse are established with the epipolar line constraint, the sequence constraint, the continuity constraint and the un-tangent constraint.

1.3 High precision positioning algorithm for wheel center

Through the stereo matching method mentioned above, the 3D coordinates of all the points on the wheel hub contour can be obtained, and then an effective algorithm based on plane projection is used to obtain the 3D coordinates of the wheel center. The detail of this algorithm is introduced in Ref. [17], and it will not be described here.

2 Experiments and Analysis

Experiments are performed on both the simulation data and the real vehicle to demonstrate the utility of the proposed method. We use the simulation data to show its effectiveness by comparing with the other methods mentioned in Refs. [6, 15], and then measure the vehicle wheelbase, the wheelbase difference and the static radius of three different vehicles to validate its accuracy. The experiments are conducted on a PC with a 2.8 GHz Intel Core 2 Duo CPU and 2 GB of memory. All the algorithms are implemented in Matlab 6.5.

2.1 Simulation experiments

In the simulation experiments, stereo images are generated by computer programming. First, two virtual cameras are designed with the same intrinsic matrix as

$$\boldsymbol{A} = \begin{bmatrix} \alpha_x & \gamma & \mu_0 \\ 0 & \alpha_y & \nu_0 \\ 0 & 0 & 1 \end{bmatrix} = \begin{bmatrix} 744.727 & 0 & 483.468 \\ 0 & 744.02 & 370.868 \\ 0 & 0 & 1 \end{bmatrix} \quad (3)$$

The intrinsic matrix contains five intrinsic parameters which are the focal length α_x and α_y in terms of pixels, the skew coefficient γ between the X and the Y axes, and the principal point μ_0 and ν_0, respectively.

Then 10 groups of different extrinsic matrices are assigned to the two virtual cameras to simulate 10 different stereo vision measurement systems. In each virtual stereo vision system, two spatial circles with the same center coordinate (100, 100, 0) and different radii which are 150 and 100 mm, respectively, are exploited as measuring objects. In order to cover all the scenarios generated by the projection of the spatial circle, the extrinsic matrices should be designed carefully.

2.1.1 Ellipse center detection experiment

10 stereo image pairs (20 images) with 1 000 × 750 resolution are generated according to the intrinsic matrix and the extrinsic matrix of 10 group virtual stereo vision systems regardless of camera distortion. In simulation images, the ellipse curve is drawn in black and the background is drawn in white. After ellipse edge detection and

the ellipse fitting process, the fitting ellipse is obtained and shown in Fig. 3, where the cross mark represents the ellipse center of the fitting ellipse and the dot mark represents the projection point of the spatial circle center (100, 100, 0) in the image plane. From Fig. 3 it is obvious that the fitting ellipse center is not consistent with the projection point of the spatial circle center. So substituting the ellipse center for the spatial circle center will cause unacceptable error, which also explains the research necessity of the proposed method.

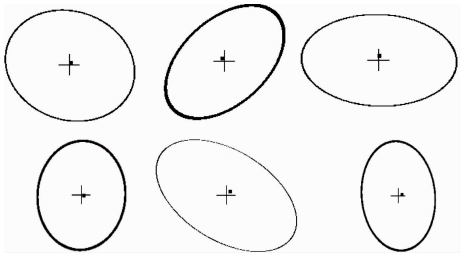

Fig. 3 Simulation images

2.1.2 Comparison of center detection experiment

Using the method described in section 1.1 and section 1.2, the ellipse edges of 10 stereo image pairs are detected, the correspondence between them is established, and the 3D coordinates of the spatial circle center O_A are calculated. In order to demonstrate the effectiveness of the proposed algorithm, our proposed method is compared with the other two algorithms.

Algorithm 1[6] The spatial circle center O_E is calculated by 3D reconstruction from the corresponding center of two fitting ellipses.

Algorithm 2[15] The spatial circle center O_S is calculated by the spatial circle fitting method with planar constraints and the Levenberg-Marquardt optimization algorithm.

Tab. 1 gives the 3D coordinates of center O_A, center O_S, center O_E and the radius of the image pair. Fig. 4 shows the error curve between center O_A, center O_S, center O_E and the true spatial circle center $O_C = (100, 100, 0)$.

Tab. 1 3D coordinates of O_A, O_S, O_E and its radius

Number	O_A		O_S		O_E	
	Coordinates	Radius/mm	Coordinates	Radius/mm	Coordinates	Radius/mm
1	(99.2, 99.6, −0.5)	151.1	(100.5, 99.4, −0.7)	148.0	(98.2, 96.5, 3.1)	145.7
2	(100.5, 99.6, 0.2)	149.3	(98.8, 100.7, 1.3)	152.3	(98.6, 96.4, 5.2)	156.4
3	(99.5, 100.1, 0.5)	150.6	(100.9, 99.3, −1.2)	152.1	(96.5, 102.3, −4.4)	155.3
4	(99.7, 99.4, 0.7)	150.8	(99.6, 100.2, −0.4)	148.2	(97.6, 97.9, −5.8)	146.7
5	(99.3, 100.8, 0.2)	149.0	(98.5, 99.4, 0.5)	152.9	(98.3, 98.0, −6.9)	146.4
6	(100.3, 100.2, −0.9)	101.4	(99.5, 99.4, 1.1)	97.8	(97.5, 104.5, 6.7)	101.3
7	(99.8, 100.4, −0.3)	98.8	(98.8, 99.2, 0.7)	101.5	(103.4, 97.2, −2.5)	95.9
8	(100.4, 99.8, 0.8)	99.1	(98.6, 99.8, −1.2)	98.6	(98.3, 97.7, 7.3)	97.0
9	(99.6, 99.7, −0.7)	101.0	(100.8, 101.2, 0.5)	97.7	(99.4, 97.9, −7.1)	105.1
10	(100.3, 99.4, 0.1)	101.7	(99.1, 99.5, −1.5)	98.2	(105.6, 99.9, −6.0)	104.8

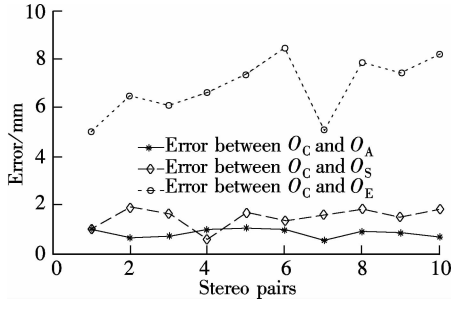

Fig. 4 Error curves of centers

Furthermore, we project the center O_C, center O_A, center O_S and center O_E to the image plane to obtain the projection points P_C, P_A, P_S, and P_E. Fig. 5 shows the error curve between P_A, P_S, P_E and P_C.

It is shown from the experimental results that no matter what 3D coordinates or the projection point of the center are, the error caused by Algorithm 1 is the biggest and the maximum error is almost 5 mm which is unacceptable, while the errors caused by our proposed algorithm and Algorithm 2 are smaller. But the Levenberg-Marquardt algorithm is a nonlinear optimization method. Algorithm 2 might fall into a local minimum, and this will cause greater errors sometimes.

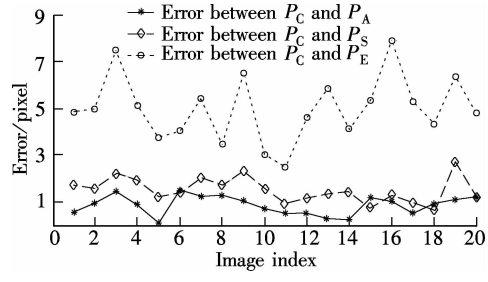

Fig. 5 Error curves of projection points

2.1.3 Time complexity experiment

Compared with Algorithm 2, the proposed method has less time complexity. In Matlab 6.5, functions "tis" and "tos" are used to record the start time and the end time of the proposed algorithm and Algorithm 2, and then the execution time can be obtained. Fig. 6 shows the average execution time (10 times) of the two algorithms for processing 10 simulation stereo pairs.

Fig. 6 shows that the execution time varies with stereo pairs, and it ranges from 25 to 30 ms in our algorithm

and from 43 to 63 ms in Algorithm 2. So the time complexity of the proposed algorithm outperforms that of Algorithm 2.

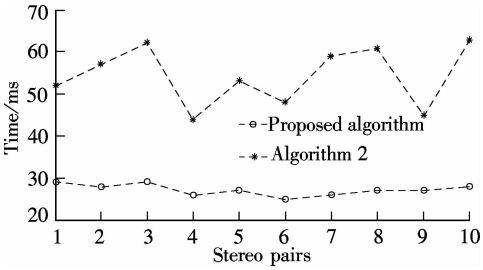

Fig. 6 Comparison of execution time

2.2 Practical experiments

In practical experiments, a Canon digital camera A75 with 3 mega pixels and 2 048 × 1 536 resolution is used as the vision sensor. The experimental objects including Roewe 550, Nissan Teana and Buick Lacrosse are measured to verify the validity of the proposed method in practice. For comparing the measurement performance, the manual measurement is done according to the following steps:

1) Wheelbase measurement

First, select the center of four wheels manually and obtain the projection points on the ground surface by suspended plumb. Then the distance between two projection points on the same side, denoted by J_{WB1} and J_{WB2}, respectively, is measured. J_{WB1} is the left wheelbase and J_{WB2} is the right wheelbase.

2) Wheelbase difference measurement

According to the wheelbase measurement, the wheelbase difference J_{WBD}, which is the difference between the left wheelbase J_{WB1} and the right wheelbase J_{WB2}, is measured.

3) Wheel radius measurement

Select the center of four wheels manually, then the distance from the four wheel centers to the ground are measured separately, denoted by $J_{JLk}(k=1,2,3,4)$. J_{JL1} is the left front wheel radius; J_{JL2} is the right front wheel radius; J_{JL3} is the left rear wheel radius; and J_{JL4} is the right rear wheel radius.

Tab. 2 shows the average results of manual measurements.

Tab. 2 Average results of manual measurements mm

Vehicle model	J_{JL1}	J_{JL2}	J_{JL3}	J_{JL4}	J_{WB1}	J_{WB2}	J_{WBD}
Roewe 550S	288	289	308	305	2702	2711	−9
Nissan Teana	309	313	329	331	2776	2781	−5
Buick Lacrosse	314	318	335	333	2839	2835	4

Before measuring by our proposed method, BMU data should be transformed into a global coordinate system by global calibration[18]. After this, we keep the four BMUs motionless and drive the car slowly to the specified location as shown in Fig. 7. Fig. 8 shows a part of the measurement scene. By our proposed method, the fitting ellipse of the wheel hub and the 3D reconstruction result of the four-wheel-hub contour and the wheel center are shown in Fig. 9.

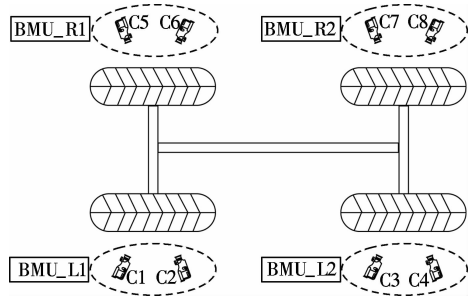

Fig. 7 Measurement system diagram

Fig. 8 Part of measurement scene

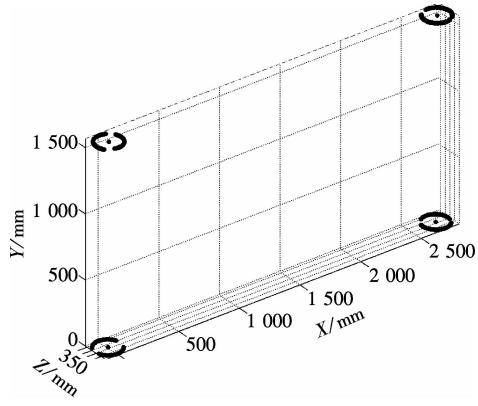

Fig. 9 3D reconstruction result

During the experiment, the process including driving the vehicle to the specified location, measuring with the proposed method and driving the vehicle off is performed 10 times. The average results are given in Tab. 3 to Tab. 5. From the experimental results, the mean absolute error (| Err |), the mean square deviation (Var) and the maximal absolute error (MaxErr) are calculated and shown in Tab. 6. The results show that our proposed method has a good reliability and little measurement error, and it is of great value in practical applications.

3 Conclusion

In practical applications, the vehicle dimension is traditionally measured manually, but it has the shortcomings of inefficiency and worse repeatability. With the development of science and technology, a measurement method

Tab. 3 Parameters of Roewe 550S measured by proposed method mm

Item	No. 1	No. 2	No. 3	No. 4	No. 5	No. 6	No. 7	No. 8	No. 9	No. 10
J_{JL1}	286.7	286.5	286.3	286.7	287.1	286.0	286.5	286.7	287.2	286.9
J_{JL2}	287.4	287.6	287.8	287.6	288.1	288.3	287.6	287.3	288.3	287.9
J_{JL3}	306.8	307.2	306.2	307.3	306.8	306.7	307.2	306.9	306.7	307.2
J_{JL4}	303.1	303.8	304.4	303.7	303.8	303.7	304.4	304.3	304.0	303.5
J_{WB1}	2 699.6	2 700.1	2 699.8	2 700.3	2 699.1	2 700.5	2 700.8	2 699.8	2 699.5	2 699.4
J_{WB2}	2 708.2	2 707.7	2 707.4	2 708.3	2 706.9	2 707.2	2 708.3	2 707.6	2 707.8	2 707.1
J_{WBD}	−8.6	−7.6	−7.6	−8	−7.8	−6.7	−7.5	−7.8	−8.3	−7.7

Tab. 4 Parameters of Nissan Teana measured by proposed method mm

Item	No. 1	No. 2	No. 3	No. 4	No. 5	No. 6	No. 7	No. 8	No. 9	No. 10
J_{JL1}	308.2	308.4	307.3	308.1	307.4	307.7	307.1	307.4	308.2	307.8
J_{JL2}	311.2	311.5	311.2	312.4	311.4	311.3	311.6	311.0	311.7	312.3
J_{JL3}	326.8	327.4	327.2	326.7	327.4	327.8	326.6	326.8	327.1	327.2
J_{JL4}	329.8	329.5	329.9	328.9	330.1	329.6	330.2	328.8	329.0	329.1
J_{WB1}	2 772.7	2 773.5	2 773.2	2 772.7	2 773.1	2 772.5	2 773.7	2 772.9	2 772.4	2 773.3
J_{WB2}	2 778.6	2 778.1	2 777.9	2 778.3	2 778.5	2 778.4	2 777.5	2 778.2	2 778.1	2 778.0
J_{WBD}	−5.9	−4.6	−4.7	−5.6	−5.4	−5.9	−3.8	−5.3	−5.7	−4.7

Tab. 5 Parameters of Buick Lacrosse measured by proposed method mm

Item	No. 1	No. 2	No. 3	No. 4	No. 5	No. 6	No. 7	No. 8	No. 9	No. 10
J_{JL1}	312.7	313.6	313.6	312.8	313.1	312.9	313.4	313.7	312.7	313.3
J_{JL2}	316.3	317.2	316.1	316.7	316.5	317.3	317.0	316.9	316.2	316.8
J_{JL3}	334.3	333.2	333.5	333.1	334.2	334.3	333.6	333.2	333.7	334.4
J_{JL4}	332.1	332.5	331.8	332.1	331.8	331.2	331.4	332.7	331.6	331.8
J_{WB1}	2 835.3	2 836.6	2 836.3	2 836.1	2 835.8	2 836.5	2 836.7	2 835.6	2 836.7	2 836.7
J_{WB2}	2 831.5	2 830.9	2 832.1	2 831.4	2 830.8	2 831.6	2 831.8	2 832.2	2 831.6	2 831.3
J_{WBD}	3.8	5.7	4.2	4.7	5	4.9	4.9	3.4	5.1	5.4

Tab. 6 $|\text{Err}|$, Var and MaxErr of experimental results mm

Item	Roewe 550S			Nissan Teana			Buick Lacrosse		
	$\|\text{Err}\|$	Var	MaxErr	$\|\text{Err}\|$	Var	MaxErr	$\|\text{Err}\|$	Var	MaxErr
J_{JL1}	1.34	0.13	2.00	1.24	0.20	1.90	0.82	0.15	1.30
J_{JL2}	1.21	0.13	1.70	1.44	0.22	2.00	1.30	0.17	1.90
J_{JL3}	1.10	0.12	1.80	1.90	0.14	2.40	1.25	0.26	1.90
J_{JL4}	1.13	0.17	1.90	1.51	0.26	2.20	1.10	0.22	1.80
J_{WB1}	2.11	0.28	2.90	3.00	0.11	3.60	2.77	0.26	3.70
J_{WB2}	3.35	0.26	4.10	2.84	0.39	3.50	3.48	0.21	4.20
J_{WBD}	1.24	0.26	2.30	0.6	0.41	1.20	0.87	0.51	1.70

based on stereo vision is presented, and the key steps are the extraction of the wheel hub contour, the matching of the wheel hub contour and the reconstruction of the wheel center. The above experiments demonstrate the utility of the proposed method in simulation and practice. The experimental results verify the validity and feasibility of the proposed method, which can substitute inefficient manual measurement for fast and economical automatic measurement.

However, the proposed method has one limitation that the performance of the proposed method depends on whether there are apparent ellipse features in the image. On the condition that the aluminum alloy wheel is not clean or the steel ring is black, the effective ellipse curve may not be located correctly, then the wheel center detection will lead to failure.

References

[1] Bian Xiaodong, Zhang Weigong, Guo Zhanjun. Vehicle dimensional parameters measuring system based on visual servoing [J]. *Measurement and Control Technology*, 2003, **22**(5): 40−42; 47. (in Chinese)

[2] Sun Lisheng, Zhu Ke. Study on visual servo measurement for vehicle geometric parameters [C]//*IEEE International Conference on Networking, Sensing and Control*. London, UK, 2007: 874−878.

[3] Bian Xiaodong. Research on vehicle dimensions measuring system based on machine vision [D]. Nanjing: School of Instrument Science and Engineering, Southeast University, 2005. (in Chinese)

[4] Su Jian, Zhai Naibin, Liu Yumei, et al. Research on vehicle dimensional measurement based on machine vision [J]. *Journal of Highway and Transportation Research and Development*, 2007, **24**(4): 145−149. (in Chinese)

[5] Bian Xiaodong, Zhang Weigong, Guo Zhanjun. Vehicle dimensions measurement based on vision servoing technology [J]. *Automotive Engineering*, 2004, **26**(3): 341 - 344. (in Chinese)
[6] Shan Hongmei, Su Jian, Zhang Libin, et al. New method for wheelbase difference detection based on stereovision [J]. *Journal of Jilin University*: *Engineering and Technology Edition*, 2010, **40**(3): 645 - 649. (in Chinese)
[7] Wei Zhenzhong, Zhang Guangjun. Distortion error model of image of ellipse center in 3D visual inspection [J]. *Journal of Beijing University of Aeronautics and Astronautics*, 2007, **24**(4): 145 - 149. (in Chinese)
[8] Li Qin, Da Feipeng, Huang Heming. An improved method of location of the circular target [C]//*International Conference on Computational Aspects of Social Networks*. Taiyuan, China, 2010: 251 - 254.
[9] Heikkil J, Silven O. A four-step camera calibration procedure with implicit image correction [C]//*Proceedings of IEEE Conference on Computer Vision and Pattern Recognition*. San Juan, Puerto Rico, 1997: 1106 - 1112.
[10] Feng J F, Shi Q Y, Chen M D. New approach for quadric curves based stereo [C]//*Proceedings of SPIE*. San Diego, CA, USA, 1995, **2573**: 190 - 195.
[11] Zhang Haopeng. Binocular stereo vision and research of pore vision measurement System [D]. Harbin: School of Electrical Engineering and Automation, Harbin Engineering University, 2009. (in Chinese)
[12] Liu Cheng, Ma Jin, Li Yibing, et al. A method for vehicle positioning based on 3-D reconstruction of spatial circle [J]. *Automotive Engineering*, 2008, **30**(8): 681 - 686. (in Chinese)
[13] Xu C X, Shi Q Y, Cheng M D. A global stereo vision method based on Wu-solver [C]//*Proceedings of GMICV*. Xi'an, China, 1995: 198 - 205.
[14] Ma Songde. Conics-based stereo motion estimation and pose determination [J]. *International Journal of Computer Vision*, 1993, **10**(1): 7 - 25.
[15] Zhang Zhifeng, Shao Shuangyun, Gao Zhan. A novel method on wheelsets geometric parameters on line based on image processing [C]//*International Conference on Measuring Technology and Mechatronics Automation*. Changsha, China, 2010: 257 - 260.
[16] Pan Xuetao, Zhang Yafeng, Meng Fei. Measurement of the geometric parameters of power contact wire based on binocular stereovision C]//*Proceedings of SPIE*. Dalian, China, 2010, **7656**: 1 - 6.
[17] Chen Xu, Lin Guoyu, Zhang Weigong. A measurement method of wheel center based on stereo vision [J]. *Journal of Nanjing University of Information Science and Technology*: *Naturel Science Edition*, 2011, **3**(1): 84 - 90.
[18] Liu Zhen, Zhang Guangjun, Wei Zhenzhong, et al. A global calibration method for multiple vision sensors based on multiple targets [J]. *Measurement Science and Technology*, 2011, **22**(12): 1 - 10.

基于立体视觉的车轮轮心检测方法

陈　旭[1]　林国余[2]

([1] 南京信息工程大学信息与控制学院, 南京 210044)
([2] 东南大学仪器科学与工程学院, 南京 210096)

摘要:由于车轮中心检测是实现车辆轮距、轮距差及车轮静立半径准确测量的关键,提出了一种基于立体视觉的车轮中心高精度检测方法. 首先,根据先验知识提取车轮轮毂的椭圆特征,并进行椭圆拟合以获取其椭圆方程. 然后,引入非相切约束条件以提高椭圆匹配的精度. 最后,采用具有低时间复杂度和高测量精度的空间圆投影方法重建车轮中心的三维坐标. 仿真实验表明,相比于椭圆中心重构法和平面约束优化法,所提方法能够更加准确地获取空间圆圆心的三维坐标. 此外,通过对3款车型的轮距、轮距差及车轮静立半径的测量实验证明了所提方法对车轮中心检测的有效性.

关键词:车轮轮心;立体视觉;3D 重建; 椭圆立体匹配
中图分类号:TP391